Role of Cytosolic Calcium Diffusion in Murine Cardiac Purkinje Cells

Bijay Limbu[1], Kushal Shah[1], Seth H. Weinberg[2] and Makarand Deo[1]

[1]Department of Engineering, Norfolk State University, Norfolk, VA, USA. [2]Department of Biomedical Engineering, Virginia Commonwealth University, Richmond, VA, USA.

Supplementary Issue: Calcium Dynamics and Cardiac Arrhythmia

ABSTRACT: Cardiac Purkinje cells (PCs) are morphologically and electrophysiologically different from ventricular myocytes and, importantly, exhibit distinct calcium (Ca^{2+}) homeostasis. Recent studies suggest that PCs are more susceptible to action potential (AP) abnormalities than ventricular myocytes; however, the exact mechanisms are poorly understood. In this study, we utilized a detailed biophysical mathematical model of a murine PC to systematically examine the role of cytosolic Ca^{2+} diffusion in shaping the AP in PCs. A biphasic spatiotemporal Ca^{2+} diffusion process, as recorded experimentally, was implemented in the model. In this study, we investigated the role of cytosolic Ca^{2+} dynamics on AP and ionic current properties by varying the effective Ca^{2+} diffusion rate. It was observed that AP morphology, specifically the plateau, was affected due to changes in the intracellular Ca^{2+} dynamics. Elevated Ca^{2+} concentration in the sarcolemmal region activated inward sodium–Ca^{2+} exchanger (NCX) current, resulting in a prolongation of the AP plateau at faster diffusion rates. Artificially clamping the NCX current to control values completely reversed the alterations in the AP plateau, thus confirming the role of NCX in modifying the AP morphology. Our results demonstrate that cytosolic Ca^{2+} diffusion waves play a significant role in shaping APs of PCs and could provide mechanistic insights in the increased arrhythmogeneity of PCs.

KEYWORDS: calcium diffusion, cardiac Purkinje cell, action potential, arrhythmias

SUPPLEMENT: Calcium Dynamics and Cardiac Arrhythmia

CITATION: Limbu et al. Role of Cytosolic Calcium Diffusion in Murine Cardiac Purkinje Cells. *Clinical Medicine Insights: Cardiology* 2016:10(S1) 17–26 doi: 10.4137/CMC.S39705.

TYPE: Review

RECEIVED: April 28, 2016. **RESUBMITTED:** June 12, 2016. **ACCEPTED FOR PUBLICATION:** June 25, 2016.

ACADEMIC EDITOR: Thomas E. Vanhecke, Editor in Chief

PEER REVIEW: Three peer reviewers contributed to the peer review report. Reviewers' reports totaled 1,188 words, excluding any confidential comments to the academic editor.

FUNDING: This work was supported in part by the American Heart Association (AHA) Scientist Development grant 12SDG11480010. The authors confirm that the funder had no influence over the study design, content of the article, or selection of this journal.

COMPETING INTERESTS: Authors disclose no potential conflicts of interest.

CORRESPONDENCE: mdeo@nsu.edu

Introduction

The cardiac Purkinje system forms a specialized electrical conduction system in the ventricles and is crucial for synchronized contraction of ventricles to maintain proper heart rhythm. The Purkinje system has been suggested to play a pivotal role in initiation and maintenance of life-threatening ventricular arrhythmias.[1–3] Recent experimental studies in transgenic mice carrying ryanodine receptor (RyR_2) mutations, typically observed in the catecholaminergic polymorphic ventricular tachycardia patients,[4] have shown that the His-Purkinje system is a major source of focal activations that initiated arrhythmia.[5,6] Experimental studies firmly suggest that action potential (AP) abnormalities in the form of early and delayed afterdepolarizations (EADs and DADs, respectively) are a more common occurrence in Purkinje cells (PCs) than in ventricular myocytes (VMs).[7] However, the exact mechanisms underlying the increased propensity to AP abnormalities in PCs are not well understood.

PCs are morphologically and electrophysiologically distinct from VMs. Specifically, T-tubules are absent in most PCs,[8,9] which results in a unique calcium (Ca^{2+}) homeostasis in PCs.[10,11] Ca^{2+} ions entering PCs via sarcolemmal (SL) channels diffuse through the cytosol to reach the sarcoplasmic reticulum (SR), before triggering Ca^{2+}-induced -Ca^{2+}-release (CICR).[12] PCs also express T-type Ca^{2+} current (I_{CaT}), absent in VMs and activating at more negative potentials than the L-type Ca^{2+} current (I_{CaL}).[13,14] As such, Ca^{2+} dynamics in PCs differs significantly from that in VMs, which may explain their increased arrhythmogeneity. Electrical excitation induces a biphasic Ca^{2+} transient in Purkinje fiber strands[15] and in isolated PCs,[12] which consists of (i) Ca^{2+} diffusion wavelets from the subsarcolemmal (subSL) region toward the central core of the cell and (ii) a focally arising Ca^{2+} wave that propagates throughout the cell.[12,16] Altered Ca^{2+} handling contributes to triggered activity,[17] and moreover, the spontaneous Ca^{2+} waves have been thought to play a role in initiating membrane depolarizations, but the mechanisms by which cytosolic Ca^{2+} diffusion alters AP morphology and potentially promotes afterdepolarizations are not well studied.

In this study, we utilized a detailed biophysical mathematical model of a murine PC to study the significant role of cytosolic Ca^{2+} diffusion waves in shaping the APs of PCs that might elucidate the mechanisms for initiating arrhythmia. The unique behavior of cytosolic Ca^{2+} diffusion in PC, as recorded in recent experiments,[16] was implemented in our model and its implications on the increased propensity of arrhythmia in PCs were investigated.

Methods

Biophysical model of a PC. In this study, the murine PC model described in the study by Vaidyanathan et al.[18] was modified to include geometrical details of a PC, described below, and extended by adding the late Na^+ current (I_{NaL}) as described in the study by Li and Rudy.[19] It has been demonstrated that I_{NaL} inactivation is a critical contributing factor in AP duration shortening in PCs during short-paced cycle lengths and alterations in I_{NaL} may contribute to EAD generation in PCs.[20]

A schematic of our PC model, including all ionic current components, buffers, and fluxes, is shown in Figure 1. The cell is assumed to be cylindrical in shape with 129 µm length and 8 µm width, based on experimentally measured dimensions of 129 ± 7 µm and 8 ± 0.3 µm, respectively.[18] Figure 1B shows the intracellular compartmentalization of the model, which is assumed to be symmetric along the length. SL currents are uniformly distributed along the length, and the SR is assumed to be in the core of the cell. RyR_2 receptors are also uniformly distributed throughout the cell.[16] The membrane currents are collected in a subSL region of 0.1 µm depth, immediately below the SL. The SR consists of two compartments: (1) a release compartment called the junctional SR (JSR), which is responsible for the release of Ca^{2+} from the SR into the cytosol (blue arrow in Fig. 1B), and (2) an uptake compartment called network SR (NSR), which is responsible for the uptake of Ca^{2+} from the cytosol into the SR (red arrow in Fig. 1B). Similar to SL, the fluxes to and from the SR are collected in a subsarcoplasmic reticulum (subSR) region of 0.1 µm depth, surrounding the SR. The radius of the SR is 2 µm and the total width of the cytosolic region is 2 µm, surrounding the SR.

Cytosolic Ca^{2+} diffusion process. A two-component cytosolic Ca^{2+} diffusion process, as observed experimentally,[12,16] was implemented in our model as follows: (1) radial diffusion of Ca^{2+} entering the cell via SL Ca^{2+} channels (I_{CaL} and I_{CaT}) propagating toward the central core (SR), referred to as wavelets, and (2) cell-wide longitudinal Ca^{2+} diffusion wave (CWW) initiated as a result of local CICRs propagating along the length of the cell. The length of the cell was divided into 10 discrete disks, with each disk possessing L- and T-type SL Ca^{2+} channels and an SR compartment, and the width of the cell was divided into 81 concentric layers, as shown in Figure 2. Cellular volume discretization enabled the simulation of longitudinal and radial Ca^{2+} diffusion processes, with a reasonable computational cost, without the necessity of representing individual Ca^{2+} release sites. The number of SR disks was constrained to 10 to minimize the computational load, while maintaining an adequate spatiotemporal Ca^{2+} resolution.

A three-dimensional diffusion equation in cylindrical coordinates was used to model the cytosolic Ca^{2+} diffusion process as follows.[21,22]

$$\frac{\partial c}{\partial t} = \beta_i(c).\left[D_{\mathrm{Car}} \frac{\partial^2 c}{\partial r^2} + D_{\mathrm{Cal}} \frac{\partial^2 c}{\partial x^2} + J_{\mathrm{Ca}} \right] \quad (1)$$

where c is the intracellular Ca^{2+} concentration, $D_{\mathrm{Car}} \frac{\partial^2 c}{\partial r^2}$ term represents the radial diffusion and $D_{\mathrm{Cal}} \frac{\partial^2 c}{\partial x^2}$ represents longitudinal diffusion. Here, D_{Cal} and D_{Car} represent the longitudinal and radial diffusion coefficients, respectively. Considering similar diffusion velocity in radial and longitudinal directions in the model, these coefficients are assumed to be equal and will be referred to as D_{Ca} ($D_{Ca} = D_{Cal} = D_{\mathrm{Car}}$). J_{Ca} is the Ca^{2+} flux from SL or SR in cytosol and $\beta_i(c)$ accounts for rapid cytosolic Ca^{2+} buffering. Finite-difference time-domain (FDTD) solution[23] was used to produce a finite and linear discretization of Equation (1) as follows:

$$\begin{aligned} \frac{dc_{(n,k,t)}}{dt} &= \beta_i(c_{(n,k,t)}) \\ &\left\{ \frac{D_{\mathrm{Car}}}{j_n(\Delta r)^2}\left[(1+j_n)c_{(n+1,k,t)} - 2j_n c_{(n,k,t)} + (j_n-1)c_{(n-1,k,t)} \right] \right. \\ &\left. + \frac{D_{\mathrm{Cal}}}{(\Delta x)^2}\left[c_{(n,k+1,t)} - 2c_{(n,k,t)} + c_{(n,k-1,t)} \right] + J_{\mathrm{Ca}(n,k,t)} \right\} \end{aligned} \quad (2)$$

where $c_{(n,k,t)}$ represents intracellular Ca^{2+} concentration at a discrete node (n,k) at a time instance t. Here, n represents the number of rows used in the model, k represents the number of columns used in the model, Δr is a small increment in the width of the model, Δx is a small increment in the length of the model, and $j_n \Delta r$ represents the spatial coordinate for concentration c_n along radial axis of cylindrical model. The flux term $J_{Ca(n,k,t)}$ at node (n,k) at a time instance t, is defined as $J_{CaSR}/V_{\mathrm{subSR}}$ for the subSR compartment, $J_{\mathrm{CaSL}}/V_{\mathrm{subSL}}$ for the subSL compartment, and zero elsewhere.

Ca^{2+} releases from the JSR compartment in the form of a RyR flux (J_{RyR}) is described as

$$J_{\mathrm{RyR}} = k_{\mathrm{RyR}}.P_{\mathrm{open}}.([Ca^{2+}]_{\mathrm{JSR}} - [Ca^{2+}]_{\mathrm{subSR}}), \quad (3)$$

and NSR Ca^{2+} uptakes via the SR Ca^{2+} ATPase (SERCA) pump (J_{SERCA}),

$$J_{\mathrm{SERCA}} = k_{\mathrm{SERCA}} \cdot \frac{V_{\mathrm{max},f}([Ca^{2+}]_{\mathrm{subSR}}/K_{mf})^H - V_{\mathrm{max},r}([Ca^{2+}]_{\mathrm{NSR}}/K_{mr})^H}{1+([Ca^{2+}]_{\mathrm{subSR}}/K_{mf})^H + ([Ca^{2+}]_{\mathrm{NSR}}/K_{mr})^H} \quad (4)$$

where $[Ca^{2+}]_x$ is the Ca^{2+} concentration in the x compartment, P_{open} is the RyR channel opening probability, k_y is the rate

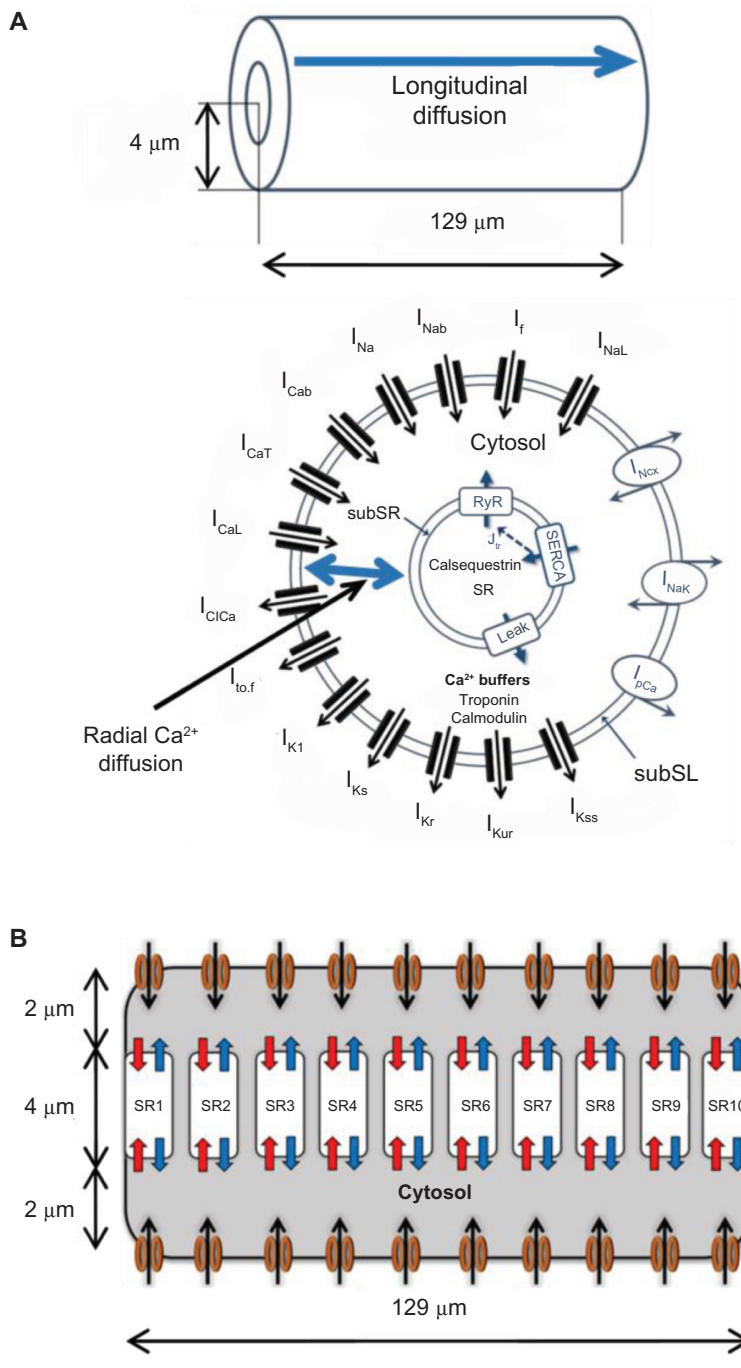

Figure 1. (**A**) Schematic showing various ionic currents and the two components of Ca^{2+} diffusion (radial and longitudinal) in the PC biophysical model. (**B**) The SR is divided into 10 discrete subcompartments (SR1–SR10) along the cell length each having its own Ca^{2+} release/uptake machinery.

for flux J_y, and K_{mf} and K_{mr} are half-saturation parameters for forward and reverse SERCA, respectively. $H = 2$ is the Hill coefficient for the SERCA pump.

A two-state Markov model of RyR gating was used in our model, consisting of an open and a closed state, with opening and closing of rates k_{open} and k_{close}, respectively, formulated as in the study by Korhonen et al.[22] The half-saturation concentration for the RyR channel, $K_{m,RyR}$, has sigmoidal dependence with $[Ca^{2+}]_{JSR}$ as given in Equation (5),

$$K_{m,\mathrm{RyR}} = 3.51\left\{1+\exp\left(\left([\mathrm{Ca}^{2+}]_{\mathrm{JSR}}-530\right)/200\right)\right\}^{-1}+0.25 \quad (5)$$

such that the RyR channel open probability (P_{open}) dynamics, governed by $[Ca^{2+}]_{subSR}$, are described as in Equation (6),

$$\frac{dP_{\mathrm{open}}}{dt} = P_{\mathrm{closed}}k_{\mathrm{open}}\left[1+\left(K_{m,\mathrm{RyR}}/[\mathrm{Ca}^{2+}]_{\mathrm{subSR}}\right)^{4}\right]^{-1} - k_{\mathrm{close}}P_{\mathrm{open}} \quad (6)$$

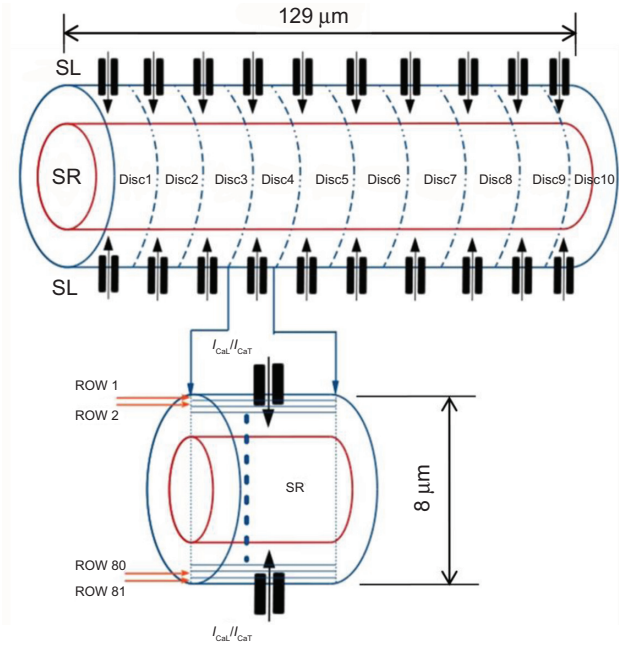

Figure 2. Implementation of spatiotemporal diffusion in the PC model. The cell is divided into 10 disks, each consisting of 81 concentric layers.

To initiate a CWW at one cell end, a $[Ca^{2+}]_{subSR}$ threshold for SR Ca^{2+} release was defined for each SR compartment, such that the SR1 threshold ($[Ca^{2+}]_{subSR} > 0.5$ µM) is less than the threshold for other compartments SR2–SR10 (0.6 µM). In a given subSR compartment, when $[Ca^{2+}]_{subSR}$ exceeded threshold, P_{open} was increased to 0.6 for a single time step ($dt = 1$ µs), triggering SR Ca^{2+} release and a rapid rise in the subSR Ca^{2+} concentration. For all other numerical integration steps, P_{open} was governed by Equation (6). The PC ionic model was paced at 1 Hz throughout the cell with stimulus current of amplitude −80 µA/µF with duration of 0.5 ms for five minutes to attain a steady state. Model parameters and values are provided in Table 1.

Results

Action potential morphology. Figure 3 shows the AP morphology obtained in our model (Fig. 3B) compared to the

Table 1. Parameters of the model.

PARAMETER	DEFINITION	VALUE
r_{SR}	Radius to the surface of SR	2 µm
r_{SL}	Radius to the surface of cell	4 µm
A_{cap}	Capacitive membrane area	7.99×10^{-5} cm^2
C_m	Specific membrane capacitance	1.0 µF/cm^2
F	Faradays constant	96.5 C/mmol
T	Temperature	308 K
R	Ideal gas constant	8.314 J/(mol K)
V_{subSR}	Volume of subSR compartment	0.082794 µL
V_{subSL}	Volume of subSL compartment	0.247012 µL

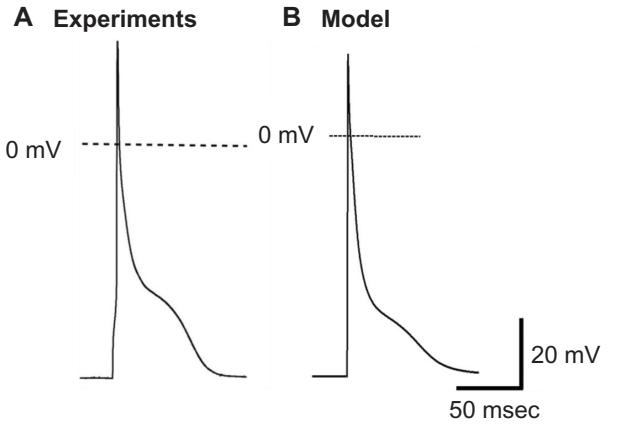

Figure 3. AP morphology (**A**) as experimentally recorded in mouse PCs[18] and (**B**) that obtained from our PC model.

experimentally recorded AP (Fig. 3A) in murine PCs.[18] Our model successfully reproduced the AP durations at 70% and 90% of repolarization (APD_{70} and APD_{90}, respectively), as well as the maximum dV/dt values obtained in the experiments (summarized in Table 2).[18] The peculiar low-voltage plateau in the mouse PC AP is apparent in the figure and was observed to be sensitive to T-type Ca^{2+} current (I_{CaT}), which is active at membrane potentials between −40 and −60 mV.[13,14] Increasing I_{CaT} magnitude resulted in more pronounced plateau (not shown), demonstrating that the I_{CaT} was responsible for the characteristic AP plateau in murine PC, in agreement with the recent findings.[18]

Intracellular Ca^{2+} diffusion. Figure 4 shows the radial and longitudinal Ca^{2+} transients observed in the PC model, clearly illustrating the biphasic nature of the Ca^{2+} transients, resulting from the two diffusion processes components. Ca^{2+} enters the cell through the SL channels (I_{CaL} and I_{CaT}) and diffuse radially toward the core of the cell where the SR is located (Fig. 4A). These radial wavelets, upon reaching the SR, trigger a CWW traveling along the length of the cell, as shown in Figure 4B. The CWWs are much higher in amplitude than the wavelets. The parameters of the average Ca^{2+} transient obtained in the model were adjusted to match the experimentally observed values reported in the study by Vaidyanathan et al.[18] Table 3 lists the characteristics of the average Ca^{2+} transients of the PC model, compared to the experimental values. The time required to attain the peak magnitude was 25 ms, and the Ca^{2+} transient decay time was 210 ms, both within the experimental ranges.

Experimental studies have suggested that a small increase in subSL Ca^{2+} can initiate the wavelets, but relatively higher Ca^{2+} threshold is needed to trigger the CWWs.[16] Figure 5 shows that Ca^{2+} diffusion waves elicited during 1 Hz pacing stimulus. During Phase 2 of the AP, Ca^{2+} enters the cell via SL channels initiating radial wavelets (arrows in Fig. 5A). When the concentration of the Ca^{2+} wavelets arriving at SR1 exceeded threshold, Ca^{2+} was released from the junctional SR1 via CICR, leading to a larger Ca^{2+} wave propagating largely

Table 2. Comparison of the AP parameters recorded in experiments with those obtained in the PC model.

PARAMETER	EXPERIMENTS	MODEL			
		SLOWER D_{Ca} = 5 μm²/ms	CONTROL D_{Ca} = 7 μm²/ms	FASTER D_{Ca} = 10 μm²/ms	FASTER D_{Ca} = 15 μm²/ms
dV/dt_{max} (mV/ms)	212 ± 15	211.34	211.39	211.43	211.44
APD_{50} (ms)	4.7 ± 0.3	7.7	7.7	7.7	7.6
APD_{70} (ms)	14.4 ± 1.6	15.6	15.5	15.7	16.4
APD_{90} (ms)	68.6 ± 5	52.99	67.29	76.39	83.69

in longitudinal direction from SR1 toward SR2 (Fig. 5B). The Ca^{2+} concentration at SR2 was thus elevated from both radial wavelets and the longitudinal Ca^{2+} wave initiated at SR1. Ca^{2+} release from junctional SR2 was triggered when the subSR Ca^{2+} concentration exceeded threshold, slightly larger than the SR1 threshold, which in turn supplements the CWW. This process was continued in subsequent SR compartments, as shown in Figure 5C–F. The magnitude of the CWW increased monotonically as it propagated from one end of the cell to the other due to contributions from the successive local CICRs.

Effects of Ca^{2+} diffusion on AP. In order to assess the effects of Ca^{2+} diffusion on the AP morphology, we studied the individual effects of Ca^{2+} wavelets and CWWs in our model.

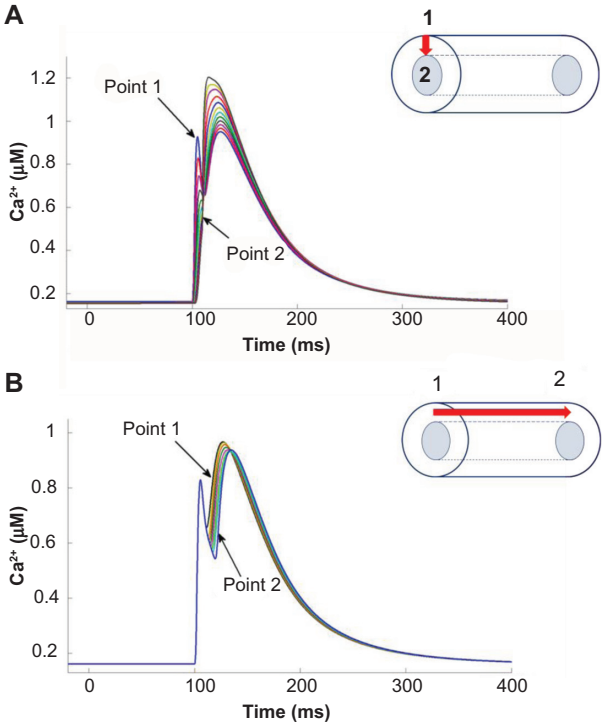

Figure 4. Cytosolic Ca^{2+} transients observed in the model representing (**A**) diffusion of radial wavelets and (**B**) longitudinal diffusion of CWW. The locations of Point 1 and Point 2 are shown on the right. The red arrow represents the component of Ca^{2+} diffusion shown.

Ca^{2+} wavelets were produced by the SL Ca^{2+} currents (I_{CaL} and I_{CaT}), without which (when both blocked) the Ca^{2+} transients were not observed. Moreover, when the CWWs were inhibited, wavelets alone were not able to produce the AP plateau (Fig. 6A). Thus, both components of Ca^{2+} diffusion process were necessary to establish the biphasic Ca^{2+} transients and reproduce the AP morphology observed in the PCs.

We next examined the influence of the effective diffusion coefficient, D_{Ca}, on AP morphology. By varying D_{Ca} we could alter the speed of the propagating Ca^{2+} transients. The baseline value of D_{Ca} in our model was chosen to be 7 μm²/ms to reproduce experimentally observed Ca^{2+} transients. This value was referenced from the study by Korhonen et al.[22], where D_{Ca} was fitted to get single effective diffusion coefficient parameter based on cytosolic Ca^{2+} propagation velocity. This value represents an effective Ca^{2+} diffusion coefficient that accounts for the influence of intracellular Ca^{2+} binding proteins or buffers, which can greatly reduce effective diffusion relative to free Ca^{2+}.[24] We found that increasing D_{Ca} produced a more pronounced plateau and significantly increased APD_{90}, and while reducing D_{Ca} to 5 μm²/ms reduced the AP plateau duration (Fig. 6B). Thus, faster Ca^{2+} transients were counterintuitively associated with more pronounced AP plateau, prompting a further investigation in the mechanisms of AP prolongation.

The average cytosolic Ca^{2+} concentration for different values of D_{Ca} is shown in Figure 7A. We found that faster Ca^{2+} transients produced larger Ca^{2+} transient amplitudes. More notable average Ca^{2+} variations were observed in the subSL compartment, which exhibited biphasic transients (Fig. 7B). The subSL Ca^{2+} concentration is mainly contributed by L-type Ca^{2+} channels, such that slower diffusion results in slower wavelet propagation, and thus large Ca^{2+} accumulation and a larger initial peak in the subSL Ca^{2+} concentration. Faster diffusion resulted in faster CICRs from each SR, ie, a smaller temporal delay between CICR events at each SR, which subsequently led to larger subSL Ca^{2+} accumulation and higher magnitude transients, observed in the second peak in the subSL Ca^{2+} concentration. These variations in cytosolic Ca^{2+} resulted in alterations in the membrane potential and various SL current magnitudes. Among the SL currents, I_{NCX}, I_{CaT}, and I_{K1} were significantly affected (Fig. 8).

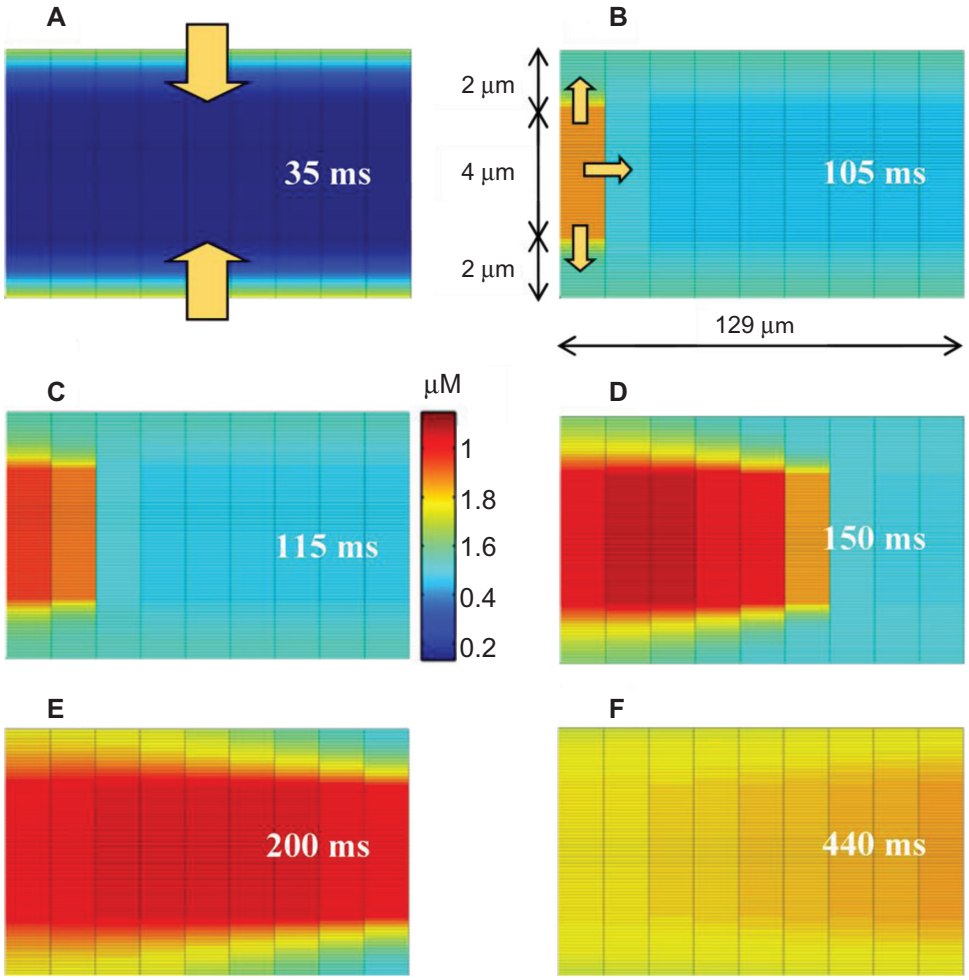

Figure 5. Propagation of Ca^{2+} transients in the PC model. (**A**) Simultaneous propagation of wavelets from SL to SR. (**B**) Initiation of CWW at SR1. (**C**), (**D**), (**E**), and (**F**) Propagation of CWW along the cell length. The arrows inside figures show direction of Ca^{2+} propagation. The time lapsed just after Ca^{2+} entered into the cell from external is also given.

We next investigated if the changes in the SL ionic currents were indeed due to variations in the subSL Ca^{2+} for different values of D_{Ca}. The subSL Ca^{2+} concentration was artificially maintained at normal levels (control case) while varying the D_{Ca} values as before. We found that the alterations in the current magnitudes as observed previously for varying D_{Ca} (Fig. 8) disappeared completely. More importantly, the variations in AP plateau were also reversed, suggesting that the variations in subSL Ca^{2+} concentration due to faster diffusion were responsible for the pronounced AP plateau.

Table 3. The parameters of average calcium transients recorded in the experiments and obtained in the model.

PARAMETER	EXPERIMENTS[18]	MODEL
Peak Amplitude	31.193 ± 0.91 AU	1.03 µM
Time to Peak	18.8 ± 13.2 ms	25 ms
Decay time	261 ± 69.18 ms	210 ms

Note: The experimental values are obtained from the study by Vaidyanathan et al.[18]

Individual contributions of I_{CaT}, I_{CaL}, and I_{NCX} in prolongation of AP plateau. We further analyzed the individual contributions of I_{CaT}, I_{CaL}, and I_{NCX} in prolongation of the AP plateau at higher values of D_{Ca}. In each case, the ionic current under consideration was artificially clamped to its normal time-dependent values as in control case (D_{Ca} = 7 µm²/ms), while varying D_{Ca} (Fig. 9). It was observed that when I_{CaT} and I_{CaL} were individually clamped to the control values, the prolongation of the AP plateau at higher D_{Ca} persisted (Fig. 9A and B), indicating insignificant contribution of these two currents in the AP prolongation. In contrast, when NCX was clamped to its control magnitude, the alterations in the AP plateau were almost reversed completely (Fig. 9C), confirming that the alterations in NCX were responsible for the prolongation of AP plateau at faster Ca^{2+} diffusion.

Discussion

In this study, we employed a detailed mouse PC model to gain understanding of Ca^{2+} propagation inside the cell and the consequences of fast and slow cytosolic Ca^{2+} transients.

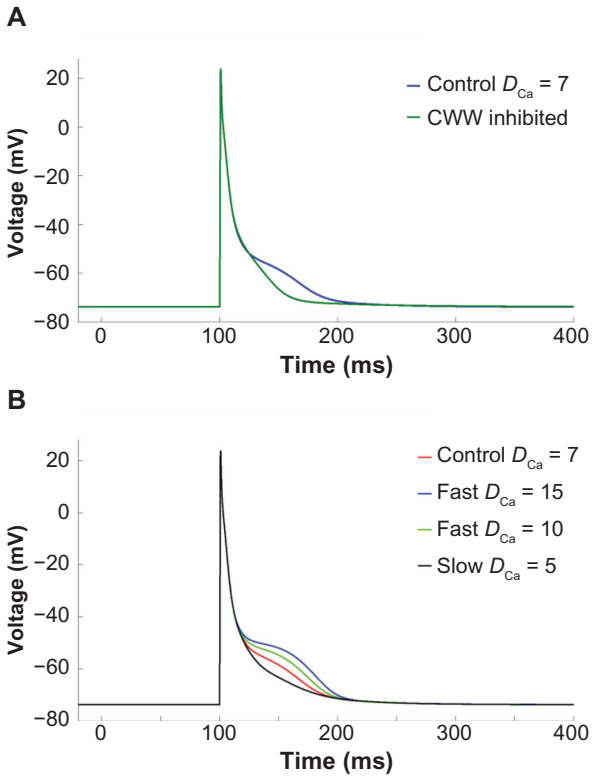

Figure 6. Ca^{2+} diffusion effect on AP. (**A**) AP plateau is disappeared when CWW is disabled. (**B**) Effect of Ca^{2+} diffusion coefficient (D_{Ca}) on AP morphology. Increasing the diffusion velocity (D_{Ca} = 10 μm²/ms and 15 μm²/ms) resulted in more pronounced plateau while slowing it (D_{Ca} = 5 μm²/ms) suppressed the plateau.

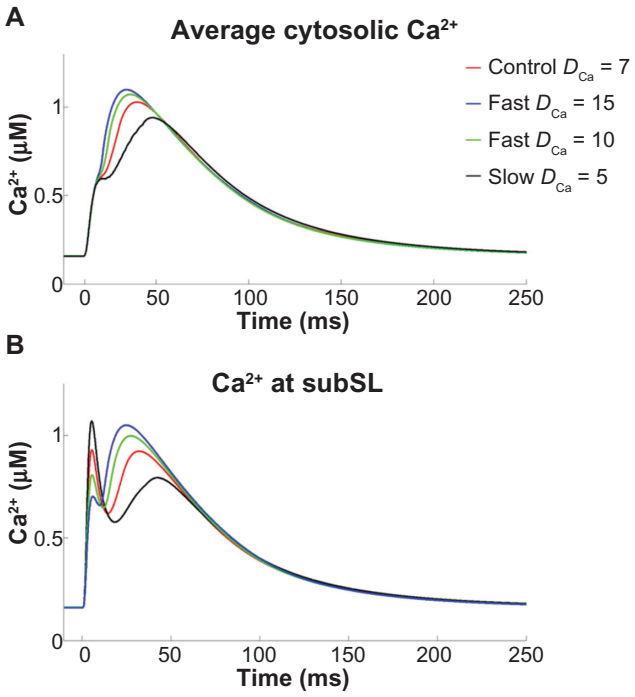

Figure 7. (**A**) Average cytosolic Ca^{2+} concentration, and (**B**) Ca^{2+} amount reaching subSL region for different values of D_{Ca}.

The spatiotemporal implementation of realistic cytosolic Ca^{2+} diffusion waves in our PC model, the first of its kind to our knowledge, provided us a unique capability to investigate the individual and combined contributions of various ionic components of a PC AP. Our main findings were: (1) during an AP, Ca^{2+} diffusion produced biphasic cytosolic Ca^{2+} transients, namely, radial wavelets and longitudinal CWWs, (2) AP plateau was specifically affected by the changes in subSL Ca^{2+} levels, (3) faster Ca^{2+} transients produced dramatic changes in subSL Ca^{2+}, which resulted in significant prolongation of the AP plateau, and (4) the prolongation of the AP plateau during faster diffusion was mediated through the inward NCX current. The low-voltage plateau phase observed in murine PCs is similarly observed in many species, including canine,[25] rabbit,[26] and human,[27] suggesting that the influence of subcellular Ca^{2+} dynamics on the plateau phase, and repolarization more generally, may be significant in other species as well.

Extensive experimental studies have demonstrated the presence of the distinct types of Ca^{2+} waves in PCs.[11,12] Stuyvers et al.[16] reported two types of Ca^{2+} transients in canine PCs: (1) Ca^{2+} transients originating directly under the sarcolemma, mostly due to influx through Ca^{2+} channels, initiating small Ca^{2+} wavelets in a region between a depth of ~6 μm under the sarcolemma and the SR, and (2) when the amplitude of these wavelets is greater than a threshold, they trigger cell-wide large Ca^{2+} waves that travel across the cell length and have much lower velocity. These Ca^{2+} waves travel at a constant velocity and with constant amplitude throughout the cell, which suggests a mechanism of Ca^{2+} diffusion boosted by local CICRs.[11,16] Our implementation of Ca^{2+} diffusion through subcellular compartmentalization satisfies these experimental observations. Because the magnitude of wavelets is lower than CWW, the possibility of wavelets alone triggering CWW is small.[12] Our mouse PC model satisfies this condition by incorporating distinct threshold values for the SR at one cell end and the remaining SR compartments. Since the SR threshold at one cell end is slightly lower, CICR is triggered by the wavelets, and the cumulative accumulation of Ca^{2+} from wavelets and the Ca^{2+} released are sufficient to subsequently trigger CICR in adjacent SR compartments. Thus, CICRs in successive compartments are triggered as the CWW propagates through the cell. The wavelets, on the other hand, propagate via diffusion between the cell periphery and the core of the cell. Spontaneous Ca^{2+} release from the SR can propagate in the reverse direction toward the membrane and may increase the local Ca^{2+} concentration in the subSL region, thereby causing membrane depolarizations through transient inward currents.[28,29]

Our results show that faster Ca^{2+} diffusion resulted in prolongation of AP plateau. When Ca^{2+} concentration in subSL region was elevated, it activated NCX to extrude Ca^{2+} ions, thus causing a net inward current. This inward I_{NCX} resulted in prolongation of the plateau. We confirmed the contribution of NCX by artificially clamping the current magnitude to its

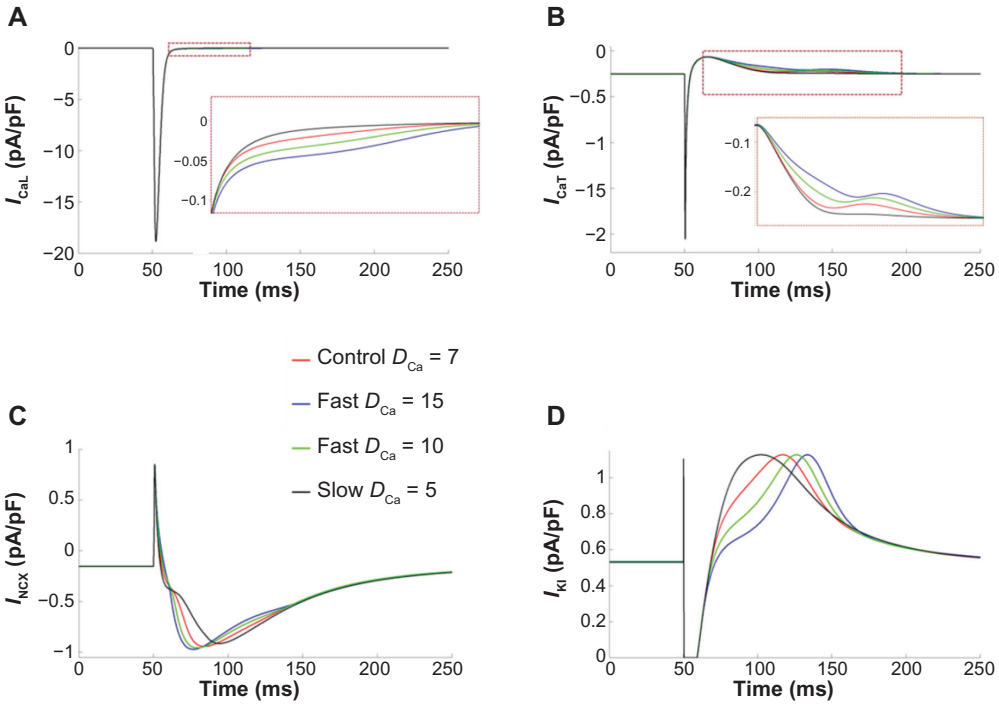

Figure 8. Ionic currents with notable variations for different D_{Ca}: (**A**) I_{CaL} – L-type Ca^{2+} current, (**B**) I_{CaT} – T-type calcium current, (**C**) I_{NCX} – sodium–Ca^{2+} exchanger current, and (**D**) I_{K1} – inward rectifier current. Insets show zoomed regions highlighted by rectangles.

control case and observing its effect on AP plateau for various Ca^{2+} diffusion velocities. Recent experiments in isoproterenol-stimulated murine VMs with RyR_2 mutations showed that random bursts of prolonged Ca^{2+} release activated NCX, which triggered low-plateau voltage EADs, with plateau voltages comparable to murine PCs.[30] Furthermore, experiments conducted using selective NCX inhibitors ORM-10103 and SEA0400 have reported successful suppression of EADs and DADs, in canine VMs and PCs.[31,32] Our results are in agreement with these experimental studies and provide further insights in the role of NCX in EAD- or DAD-induced arrhythmias originated in PCs.

Limitations. Our model assumes that the SR is situated symmetrically at the center of the cell and is uniformly divided into 10 subcompartments. The exact location and distribution of the SR in PCs is largely unknown and warrants further experimental evidence to faithfully implement it. Further, our model does not differentiate between the Ca^{2+} release mechanisms of IP_3 receptors and ryanodine (RyR_2 and RyR_3) receptors as suggested in the study by Stuyvers et al.[16] Instead, a basic two-dimensional spatiotemporal diffusion was implemented in our model to study the effects of collective cytosolic Ca^{2+} diffusion. Finally, our model does not account for the influence of stochasticity in RyR gating and fluctuations driven by stochastic Ca^{2+} release.[33–37] As highlighted in the studies by Stuyvers et al.[16] and Boyden et al.[12], the biphasic nature of Ca^{2+} transients involves both spatial aspects of Ca^{2+} diffusion and spontaneous SR Ca^{2+} release. In order to avoid the complexity and variability of a stochastic model, we artificially triggered SR Ca^{2+} release from one cell end, such that we could focus on the regulatory role of Ca^{2+} diffusion in Ca^{2+} dynamics and subsequent influence on electrophysiology. Future work will investigate these issues by incorporating a stochastic RyR gating model for SR Ca^{2+} release. Notwithstanding these limitations, the model was able to reproduce the experimental observations and provided significant insights in the role of Ca^{2+} diffusion in shaping the AP of PCs.

Conclusions

The study used a morphologically detailed numerical model of murine PC integrated with a spatiotemporal cytosolic Ca^{2+} diffusion process to study a possible mechanism of AP abnormalities, which could lead to arrhythmia. The PC model successfully reproduced the distinct Ca^{2+} dynamics and the AP morphology reported in experiments. It was observed that cytosolic Ca^{2+} diffusion waves in PCs characterized their peculiar AP morphology. The faster Ca^{2+} diffusion produced biphasic transients in the subSL region, which led to the prolongation of the AP plateau. Detailed analysis revealed that the AP prolongation at faster diffusion was mediated via inward NCX current. Our simulation results provide valuable insights in the mechanisms of increased propensity to AP abnormalities in cardiac PCs when compared to VMs.

Author Contributions

Performed the modeling and simulations, and wrote the first draft of the manuscript: BL. Developed the initial model formulations and design: KS. Reviewed the work and made

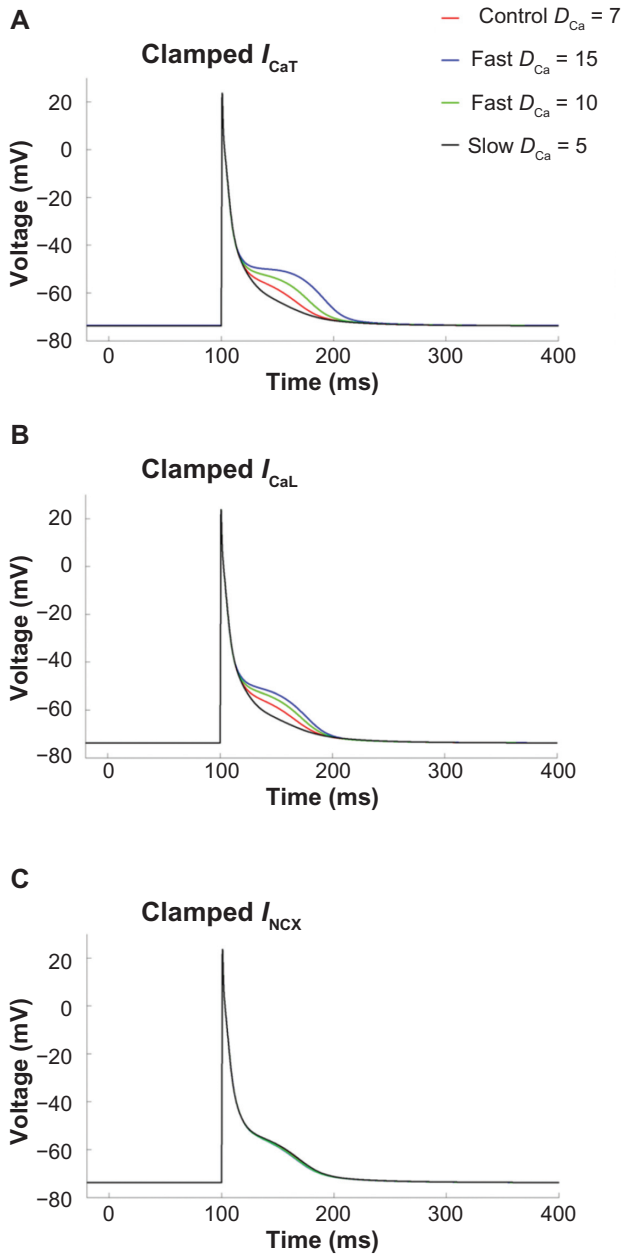

Figure 9. APs when (**A**) I_{CaT}, (**B**) $I_{CaL,}$ and (**C**) I_{NCX} were individually clamped to control values during varying D_{Ca}. Note that the AP prolongation was completely reversed in (**C**).

critical revisions to the manuscript: SHW. Conceived the design of the study, made critical revisions to the manuscript, and approved the final version: MD. All the authors reviewed and approved the final manuscript.

REFERENCES

1. Betts JG. *Anatomy & Physiology*. Houston, TX: OpenStax College, Rice University; 2013.
2. Nogami A. Purkinje-related arrhythmias part I: monomorphic ventricular tachycardias. *Pacing Clin Electrophysiol*. 2011;34(5):624–50.
3. Nogami A. Purkinje-related arrhythmias part II: polymorphic ventricular tachycardia and ventricular fibrillation. *Pacing Clin Electrophysiol*. 2011;34(8):1034–49.
4. Leenhardt A, Lucet V, Denjoy I, Grau F, Ngoc DD, Coumel P. Catecholaminergic polymorphic ventricular tachycardia in children. A 7-year follow-up of 21 patients. *Circulation*. 1995;91(5):1512–9.
5. Cerrone M, Noujaim SF, Tolkacheva EG, et al. Arrhythmogenic mechanisms in a mouse model of catecholaminergic polymorphic ventricular tachycardia. *Circ Res*. 2007;101(10):1039–48.
6. Priori SG, Napolitano C, Memmi M, et al. Clinical and molecular characterization of patients with catecholaminergic polymorphic ventricular tachycardia. *Circulation*. 2002;106(1):69–74.
7. Herron TJ, Milstein ML, Anumonwo J, Priori SG, Jalife J. Purkinje cell calcium dysregulation is the cellular mechanism that underlies catecholaminergic polymorphic ventricular tachycardia. *Heart Rhythm*. 2010;7(8):1122–8.
8. Sommer JR, Johnson EA. Cardiac muscle. A comparative study of Purkinje fibers and ventricular fibers. *J Cell Biol*. 1968;36(3):497–526.
9. Di Maio A, Ter Keurs HE, Franzini-Armstrong C. T-tubule profiles in Purkinje fibres of mammalian myocardium. *J Muscle Res Cell Motil*. 2007;28(2–3):115–21.
10. Boyden PA, Hirose M, Dun W. Cardiac Purkinje cells. *Heart Rhythm*. 2010;7(1):127–35.
11. Ter Keurs HEDJ, Boyden PA. Calcium and arrhythmogenesis. *Physiol Rev*. 2007;87(2):457–506.
12. Boyden PA, Pu J, Pinto J, Keurs HE. Ca(2+) transients and Ca(2+) waves in Purkinje cells: role in action potential initiation. *Circ Res*. 2000;86(4):448–55.
13. Vassort G, Talavera K, Alvarez JL. Role of T-type Ca2+ channels in the heart. *Cell Calcium*. 2006;40(2):205–20.
14. Niwa N, Yasui K, Opthof T, et al. Cav3.2 subunit underlies the functional T-type Ca2+ channel in murine hearts during the embryonic period. *Am J Physiol Heart Circ Physiol*. 2004;286(6):H2257–63.
15. Wier WG, Isenberg G. Intracellular [Ca2+] transients in voltage clamped cardiac Purkinje fibers. *Pflugers Arch*. 1982;392(3):284–90.
16. Stuyvers BD, Dun W, Matkovich S, Sorrentino V, Boyden PA, ter Keurs HE. Ca2+ sparks and waves in canine Purkinje cells: a triple layered system of Ca2+ activation. *Circ Res*. 2005;97(1):35–43.
17. Santulli G, Marks AR. Essential roles of intracellular calcium release channels in muscle, brain, metabolism, and aging. *Curr Mol Pharmacol*. 2015;8(2):206–22.
18. Vaidyanathan R, O'Connell RP, Deo M, et al. The ionic bases of the action potential in isolated mouse cardiac Purkinje cell. *Heart Rhythm*. 2013;10(1):80–7.
19. Li P, Rudy Y. A model of canine Purkinje cell electrophysiology and Ca(2+) cycling: rate dependence, triggered activity, and comparison to ventricular myocytes. *Circ Res*. 2011;109(1):71–9.
20. Iyer V, Roman-Campos D, Sampson KJ, Kang G, Fishman GI, Kass RS. Purkinje cells as sources of arrhythmias in long QT syndrome type 3. *Sci Rep*. 2015;5:13287.
21. Crank J. *The Mathematics of Diffusion*. Oxford: Clarendon Press; 1979.
22. Korhonen T, Hänninen SL, Tavi P. Model of excitation-contraction coupling of rat neonatal ventricular myocytes. *Biophys J*. 2009;96(3):1189–209.
23. Sadiku MNO. Numerical Techniques in Electromagnetics, 2nd ed. CRC Press; 2000. Boca Raton, FL
24. Wagner J, Keizer J. Effects of rapid buffers on Ca2+ diffusion and Ca2+ oscillations. *Biophys J*. 1994;67(1):447–56.
25. Zaza A, Malfatto G, Rosen MR. Electrophysiologic effects of ketanserin on canine Purkinje fibers, ventricular myocardium and the intact heart. *J Pharmacol Exp Ther*. 1989;250(1):397–405.
26. Dumaine R, Cordeiro JM. Comparison of K+ currents in cardiac Purkinje cells isolated from rabbit and dog. *J Mol Cell Cardiol*. 2007;42(2):378–89.
27. Lee FY, Wei J, Wang JJ, Liu H, Shih T, Lin CI. Electromechanical properties of Purkinje fiber strands isolated from human ventricular endocardium. *J Heart Lung Transplant*. 2004;23(6):737–44.
28. Ferrier GR. The effects of tension on acetylstrophanthidin-induced transient depolarizations and aftercontractions in canine myocardial and Purkinje tissues. *Circ Res*. 1976;38(3):156–62.
29. Kass RS, Tsien RW, Weingart R. Ionic basis of transient inward current induced by strophanthidin in cardiac Purkinje fibres. *J Physiol*. 1978;281:209–26.
30. Zhao YT, Valdivia CR, Gurrola GB, et al. Arrhythmogenesis in a catecholaminergic polymorphic ventricular tachycardia mutation that depresses ryanodine receptor function. *Proc Natl Acad Sci U S A*. 2015;112(13):E1669–77.
31. Jost N, Nagy N, Corici C, et al. ORM-10103, a novel specific inhibitor of the Na +/Ca 2+ exchanger, decreases early and delayed afterdepolarizations in the canine heart. *Br J Pharmacol*. 2013;170(4):768–78.
32. Nagy N, Kormos A, Kohajda Z, et al. Selective Na(+)/Ca(2+) exchanger inhibition prevents Ca(2+) overload-induced triggered arrhythmias. *Br J Pharmacol*. 2014;171(24):5665–81.
33. Weinberg SH, Smith GD. Discrete-state stochastic models of calcium-regulated calcium influx and subspace dynamics are not well-approximated by ODEs that neglect concentration fluctuations. *Comput Math Methods Med*. 2012;2012:897371.

34. Wang X, Hao Y, Weinberg SH, Smith GD. Ca(2+)-activation kinetics modulate successive puff/spark amplitude, duration and inter-event-interval correlations in a Langevin model of stochastic Ca(2+) release. *Math Biosci*. 2015;264:101–7.
35. Ji H, Li Y, Weinberg S. Calcium ion fluctuations alter channel gating in a stochastic luminal calcium release site model. *IEEE/ACM Trans Comput Biol Bioinform*. 2015. doi: 10.1109/TCBB.2015;PP(99):1–9.
36. Rüdiger S, Shuai JW, Huisinga W, et al. Hybrid stochastic and deterministic simulations of calcium blips. *Biophys J*. 2007;93(6):1847–57.
37. Thul R, Coombes S, Roderick HL, Bootman MD. Subcellular calcium dynamics in a whole-cell model of an atrial myocyte. *Proc Natl Acad Sci U S A*. 2012;109(6):2150–5.